Supporting Information

Zell et al. 10.1073/pnas.1315991111

SI Appendix

Dynamic Strain and Frequency Sweep of SDS Surfaces

To rule out the possibility of a nonlinear response of the SDS solution surfaces, we performed a strain sweep measurement (~0.01–0.3 rad, 1 Hz) and a frequency sweep measurement (0.1–10 Hz, $\Delta\theta_0 < 0.07$ rad) using a 50-μm microbutton. Fig. S1 reveals no dependence of ζ_R on $\Delta\theta_0$ or f. Moreover, for both 3- and 10-mM SDS, ζ_R^{rel} is O(1), indicating the measurement is dominated by the underlying subphase.

Surface Flow Visualization

We prepare custom silica particle tracers, following a procedure similar to Kulkarni et al. (1). First, 0.15 g of silica particles (radius = 2.54 μm, Bangs Labs) were dried at 120 °C for 1 h, then rendered hydrophobic by dispersing in 15 mL of toluene containing 1% trichloro(1H,1H,2H,2H-perfluorooctyl)silane. After mixing with a stir bar for 2 h, particles were washed with toluene and isopropyl alcohol six times each, before dispersing in isopropyl alcohol.

After adding a microbutton to the liquid substrate, ~1 μL of hydrophobized silica tracer solution was deposited using a microliter syringe. We visualized the surface flow field during oscillatory microbutton measurements of $\zeta_R^*(\omega)$ at 1 Hz by recording images of the probe and surrounding flow tracers. The particle positions were tracked using a MATLAB algorithm adapted from Crocker and Grier (2). The normalized azimuthal velocity was calculated from $\Delta\theta_0$ of the microbutton and the amplitude of the angular displacement of each particle relative to the microbutton center, and the normalized distance of each particle from the microbutton center. Fig. 3*C* shows the averaged normalized velocity averaged in concentric rings extending from the radius of the probe, each 3 pixels thick.

Microbutton Translation Experiments

Calibration and Operation. Each individual electromagnet establishes a field strength gradient that depends on position (Fig. S2*A*), with field strength (and gradient) decaying with distance from the magnet. The microbutton is forced toward one electromagnet by running a current through that electromagnet's coils, then in the opposite direction with a current through the other electromagnet's coils, keeping the microbutton within a 500-μm location. The velocity is measured in forward and reverse directions,

$$U_{F,R} = \frac{m \cdot \nabla B_{F,R}}{\zeta_T}, \qquad \text{[S1]}$$

and the two results averaged, giving

$$|U| = \frac{m \cdot \nabla \langle |B| \rangle}{\zeta_T}. \qquad \text{[S2]}$$

Over the central ±1.5 mm where measurements are taken, the magnitude of the magnetic field gradient $|\nabla B| \sim 11.0 \pm 0.3$ G/mm is relatively constant, allowing ζ_T to be determined via

$$\zeta_T = \frac{m \cdot \nabla \langle |B| \rangle}{\langle |U| \rangle}. \qquad \text{[S3]}$$

On a clean air–water surface, the hydrodynamic drag force on the probe can be quantified using the thin-disk limit of the translational drag coefficient due to an underlying viscous subphase (Eq. **6**) and the measured average velocity via

$$|F_H| = \frac{16\eta a}{3} \langle |U| \rangle. \qquad \text{[S4]}$$

Fig. S2*B* shows that the hydrodynamic force is in balance with the externally applied force ($F_{\text{mag}} = m \cdot \nabla B$) for different microbutton types and thus magnetic moments (m).

Translation Within Eicosanol Monolayers. Rotating microbutton measurements reveal a well-resolved, Newtonian-like surface shear viscosity for eicosanol monolayers in the $L_{S,I}$ phase (Fig. 4). At $\Pi \sim 35.5$ mN/m (Fig. S3), oscillatory shear measurements with a 10-μm microbutton give Bo ~ 10^3, whereas translational drag measurements give $\zeta_T/\zeta_{T,\text{clean}} \sim 700$, of O(Bo) and in relatively good agreement with Eq. **8**.

1. Kulkarni SA, Ogale SB, Vijayamohanan KP (2008) Tuning the hydrophobic properties of silica particles by surface silanization using mixed self-assembled monolayers. *J Colloid Interface Sci* 318(2):372–379.

2. Crocker JC, Grier DG (1996) Methods of digital video microscopy for colloidal studies. *J Colloid Interface Sci* 179(1):298–310.

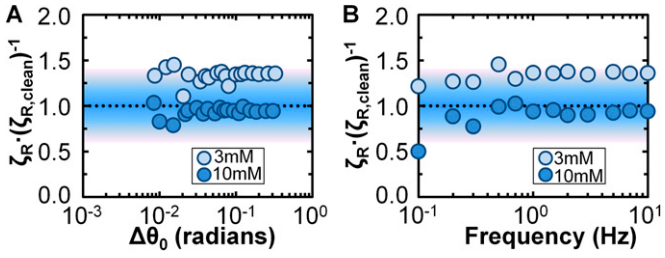

Fig. S1. (*A*) Dynamic strain sweep at 1 Hz using 50-μm microbutton at SDS solution surfaces shows ζ_R to be strain-independent and O(1), indicating subphase-dominant behavior. (*B*) Dynamic frequency sweep at strain amplitudes <0.07 rad also indicates bulk-dominated rheology.

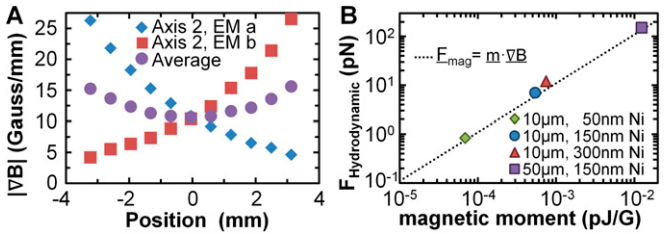

Fig. S2. (*A*) Magnetic field strength gradients driven by 1 A current, derived from the *B* field measured along the electromagnet axis, as a function of distance from the sample center. Each electromagnet ("a" and "b") establishes a field strength gradient that decays with distance from the magnet, with an average that is insensitive to position near the center of the sample cell. Translation experiments are performed within 1.5 mm of the center, wherein field strength gradients vary by less than 15%. (*B*) Hydrodynamic force on different microbutton types, extracted from measured translational velocity, plotted against magnetic moments measured via rotation.

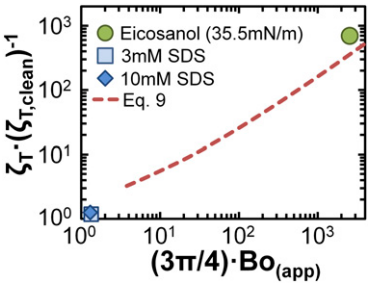

Fig. S3. Measured ζ_T on surfactant monolayers, normalized by ζ_T on an air–water surface plotted against the apparent Boussinesq number measured from rotational (pure shear) experiments. When surface drag truly dominates (Bo >> 1), the normalized drag is large (ζ_T^{rel} >> 1). By contrast, translational drag measurements on SDS are also consistent with subphase-dominated (i.e., inviscid) surface shear rheology.

Table S1. Microbutton surface shear rheology of various soluble surfactants

Surfactant	Type	Concentration	$\zeta_R/\zeta_{R,\ clean}$ 10 μm	10 μm, R	50 μm
SDS (SDS)	Anionic	1 mM	0.9	1.0	0.9
		3 mM	0.8	1.1	0.8
		6 mM	1.5	1.4	0.9
		10 mM	1.0	1.3	0.9
		20 mM	1.3	1.3	1.1
Sodium 1-dodecanesulfonate	Anionic	0.3 mM	0.9	—	—
		1 mM	1.2	—	—
		3 mM	0.9	—	—
Cetyltrimethylammonium bromide (CTAB)	Cationic	0.3 mM	—	—	1.0
		1 mM	—	—	1.1
		3 mM	—	—	1.0
TERGITOL 15-S-9	Nonionic	0.1 wt %	—	—	1.0
TERGITOL 15-S-20	Nonionic	0.1 wt %	—	—	0.9
TERGITOL L-62	Polymeric	0.1 wt %	—	—	0.8
TERGITOL XH	Polymeric	0.1 wt %	—	—	0.8
TERGITOL Nonidet P-40	Nonionic	0.1 wt %	—	—	0.9
TRITON CG-110	Nonionic	0.2 wt %	—	—	0.9
ECOSURF SA-7	Nonionic	0.1 wt %	1.1	—	1.4
ECOSURF SA-9	Nonionic	0.1 wt %	—	—	0.9
ECOSURF SA-15	Nonionic	0.1 wt %	1.1	—	0.9
ECOSURF EH-6	Nonionic	0.1 wt %	—	—	1.2
ECOSURF EH-9	Nonionic	0.1 wt %	—	—	1.1
ECOSURF EH-40	Nonionic	0.1 wt %	—	—	1.2
Triton CF-76	Nonionic	0.1 wt %	—	—	1.1
Triton DF-12	Nonionic	0.1 wt %	—	—	1.1
Triton X-100	Nonionic	0.1 wt %	—	—	1.3
Tween 20	Polymeric	0.1 wt %	—	—	1.0
Tween 80	Polymeric	0.1 wt %	—	—	1.1
Brij L23	Polymeric	0.1 wt %	—	—	1.1
Linear alkylbenzene sulfonic acid (LABSA)	Anionic	0.1 wt %	—	—	1.2
Sodium dodecylbenzenesulfonate (SDBS)	Anionic	0.1 wt %	—	—	1.2
F-108	Polymeric	0.1 wt %	—	—	1.0

Microbutton surface shear rheology reveals soluble surfactants of various type (e.g., ionics, nonionics) to be surface shear inviscid, undercutting evidence for a correlation between surface shear rheology and foam stability. The relative rotational drag coefficient ($\zeta_R/\zeta_{R,clean}$) using probes of various size and shape is measured to be order one and implies the surface shear rheology is immeasurably low for a wide range of surfactants with varying composition (anionic, cationic, non-ionic and polymeric) and foamability, with high foamers like SDS; moderate foamers like Tergitol 15-S-9, 15-S-20, Nonidet P-40 and Ecosurf SA-9 and SA-15; and low foamers like Tergitol L-62 and XH, Ecosurf EH-6 and EH-9, and Triton CF-76 and DF-12.

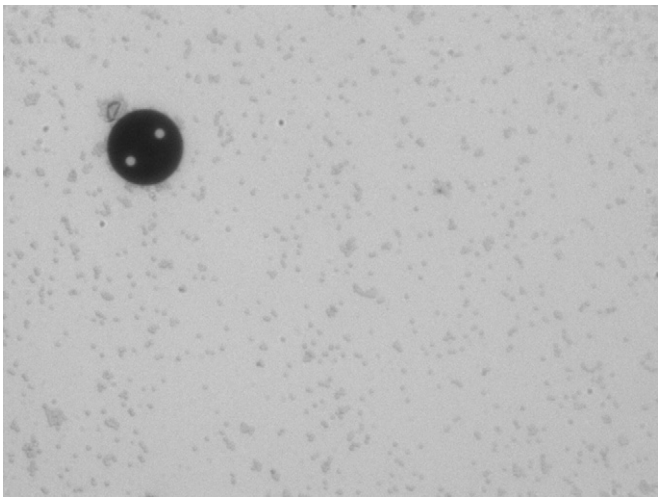

Movie S1. Particle-tracking video microscopy of the interfacial deformation field around a 50-micron microbutton oscillating within the interface of a 10mM SDS solution, corresponding to Fig. 3*A*. Particle adsorption increases the effective radius of the microbutton by several particle diameters, but does not affect the r^{-2} decay characteristic of subphase-dominated (surface shear inviscid) deformations (Fig. 3*C*).

Movie S1

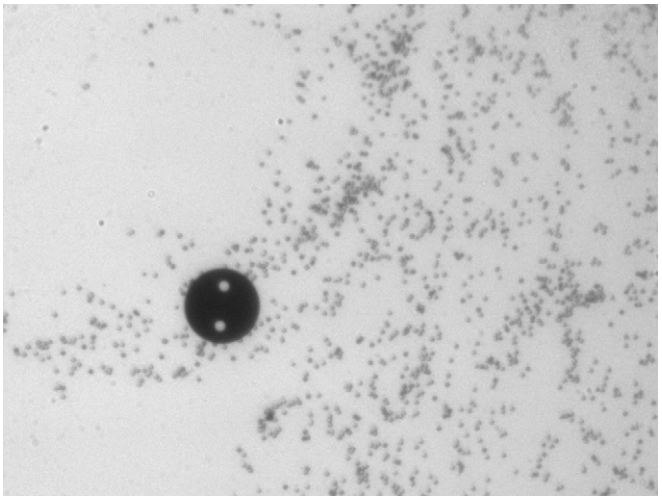

Movie S2. Particle-tracking video microscopy of the interfacial deformation field around a 50-micron microbutton oscillating within a 20mN/m eicosanol monolayer, corresponding to Fig. 3*B*. Particle adsorption increases the effective radius of the microbutton by about one-particle diameters, but does not affect the r^{-1} decay characteristic of interfacially dominated (surface shear viscous) deformations (Fig. 3*C*).

Movie S2